HEFAT2014
10th International Conference on Heat Transfer, Fluid Mechanics and Thermodynamics
14 – 16 July 2014
Orlando, Florida

THERMOREFLECTANCE OF CARBON NANOFIBERS: JOULE HEATING EXPERIMENT AND CALIBRATION

Shawn Tokairin[1], Kevin Read[2], Patrick Wilhite[2], Jason Chen, Drazen Fabris[1]*, Cary Y. Yang[2],
*Author for correspondence
Center for Nanostructures, Dept. of Mechanical Engineering[1], Dept. of Electrical Engineering[2],
Santa Clara University,
California 95050
USA
E-mail: dfabris@scu.edu

ABSTRACT

Thermoreflectance (TR) is a novel, non-contact technique that uses the change in surface reflectivity over optical wavelengths of light to deduce temperature. This reflectivity is also wavelength dependent and material dependent. By calibrating a sample to determine the TR coefficient k, the relative change in intensity per degree change in temperature, the difference between heated and cool images is used to measure the relative temperature change. A two-dimensional, steady state TR method is used to examine the thermoreflectance behavior of carbon nanofibers (CNFs). Signal mixing between the CNF and the substrate at the sub-micron level is minimized by use of gold at its TR cross-point. A TR signal is created by the CNF as it is subject to Joule heating by passing a constant current through it. The calibration coefficient is measured though uniform heating of the sample. Initially, imaging during the heating process suffered from image shifting caused by air currents. Once the visible shifting is removed, the TR coefficient k_{comp} derived from the heating experiment was 7.93×10^{-5}/K. To validate these results, the TR signal from a CNF undergoing Joule heating and the predicted temperature from a heat-transfer model were used to produce a second calibration, yielding a TR coefficient k_{Joule} of 2.45×10^{-5}/K. The discrepancy between the two TR coefficients suggests that further experiments are needed to determine more accurately the CNF TR coefficient.

INTRODUCTION

With new designs for integrated circuits, the line width and interconnect via size are shrinking. This leads to an increased proportion of the energy being dissipated through interconnects which can result in a greater potential for electromigration and thermally induced failure [1]. Due to their ease of manufacture and good electrical and thermal characteristics, carbon nanofibers are currently being investigated as an interconnect replacement for copper in microelectronics [2]. In evaluating this new material, it is important to determine the electrical properties, the amount of heating and location of heating, and failure mechanisms. For a detailed understanding, an in-situ method of temperature measurement is necessary. Thermoreflectance offers a method to measure thermal properties of materials at these small scales.

NOMENCLATURE

Mechanical

ρ		Optical Reflectivity
T	[K]	Temperature
R		Reflected Intensity
k	[1/K]	Thermoreflectance coefficient
k	[W/m K]	Thermal conductivity
ω	[m^2]	Cross-sectional area
l	[m]	Half-length of CNF
x	[m]	Distance from CNF center
a	[$1/m^2$]	Dissipation coefficient
f	[K/m^2]	Generation coefficient
γ	[W/m]	Thermal dissipation per length

Electrical

σ	[Ω/m]	Electrical Conductivity
R	[Ω]	Electrical Resistance
P	[W]	Electrical Power
I	[Amps]	Electrical Current

Subscripts

CNF	Carbon Nanofiber
e,c	Electrical contact (resistance)
0	Ambient
Joule	Derived from Joule heating experiment
Comp	Derived from broad heating experiment and shifting compensated
Raw	Derived from broad heating experiment and no shifting compensation
sub	The substrate below the suspended CNF
t,c	Thermal contact (resistance)

It has become increasingly important to develop new techniques to measure temperature at the sub-micron level. Traditional methods such as thermocouples no longer work at this scale due to their relatively large size and necessary contact with the sample. Instead, non-contact techniques are being developed to circumvent these limitations. Scanning Thermal Microscopy (ShTM) and Near Field Optical Microscopy (NSOM) are two such techniques that rely on visible light, but both of these techniques only provide localized measurements [3]. Thermoreflectance offers a 2-D, steady-state technique with a relatively high level of accuracy to measure temperature at the micron and sub-micron scales.

The methods used by Yang *et al.* [4] and Balandin *et al.* [5] indirectly measure the thermal properties of CNFs and graphene. In the experiment by Yang *et al.*, the measurement of the CNF's thermal conductivity relies on separating the contact resistance from the CNF's thermal conductance. In the experiment by Balandin *et al.*, the indirect temperature measurement of a single point is dependent on the spatial accuracy and the uniformity of the graphene. The 2-D measurements taken by the Thermal Imaging Systen (ThIS) offer the ability to measure the local temperature profile of the CNFs and the contact heating. These advantages offer the ability to directly measure thermal conductivity and contact resistance.

Thermoreflectance uses a temperature-driven change in reflectivity of a material to extract a temperature measurement. The reflectivity of a material is dependent on wavelength and temperature. It is assumed that the reflectivity has a small, linear dependence on temperature so that

$$\rho(T_0 + \Delta T) \cong \rho_0 \cdot (1 + k\Delta T) \qquad (1)$$

where ρ is the material's reflectivity, T is temperature, and k is the material's thermoreflectance coefficient. For greater sensitivity, the measurement takes two images of a sample: one at an elevated temperature and one at ambient conditions. These measurements are taken in alternating sequence to average out other effects such as variation in the incoming light intensity. The temperature of a sample is calculated from the difference in the means of the high temperature and ambient temperature measurements so that

$$\Delta T = \frac{1}{k}\frac{\Delta R}{R} \qquad (2)$$

where R is the reflected intensity of the sample. In order to measure temperature, the TR coefficient k is needed. This coefficient must be determined from a calibration of the specific sample because the coefficient will vary with surface finish, the layer thickness and purity of the material. Thermoreflectance offers a way to directly measure the temperature, and thus thermal performance, of CNFs.

Measurement of CNF temperature poses several challenges. The CNF structure is very small with diameters of 100 nm as measured with a Hitachi S-4800 SEM. The cylindrical surface of the CNF will change the characteristics of the light-surface interaction. The material thermoreflectance coefficient is not well known. Thus, the TR coefficient for the CNF is derived from the reflection off of its curved surface. In addition to these, the CNF must be supported on a substrate. Due to its size, the CNF and substrate signal is mixed in the detection. For the experiments, gold electrodes are used. Gold has a well-documented TR response in the optical range as measured by Beran and by Burzo *et al.* [6, 7]. Due to the small size of the CNFs, diffraction will create signal mixing between the gold and the CNFs. In order to minimize this effect, a characteristic of gold TR behavior is used. Gold's TR coefficient k approaches zero at an illumination wavelength of 500 nm. This is different than the overall reflectivity ρ, which is non-zero. By illuminating the sample with 500 nm light, the strength of the signal from the CNFs is substantially stronger than the TR signal from the gold. At 500 nm illumination, the TR coefficient for gold is $-3 \cdot 10^{-5}$ [6]. The spatial broadening of the CNF image remains and is due to diffraction.

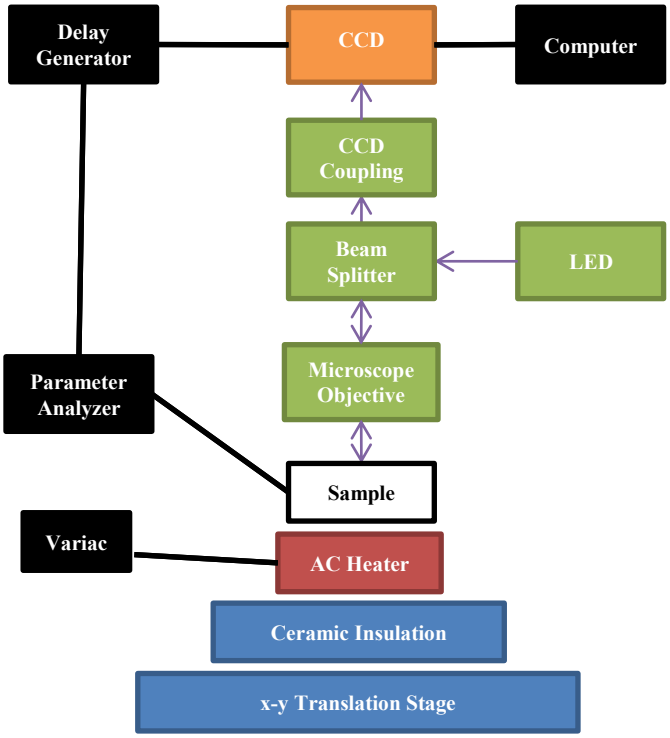

Figure 1: Layout of the Thermoreflectance Imaging System as developed by the Center for Nanostructures at Santa Clara University.

ThIS, developed in-house by the Center for Nanostructures at Santa Clara University, uses a microscope-mounted CCD to take TR measurements. The schematic of the components of ThIS can be seen in Figure 1. Prior work has used this system to measure the contact resistance of thin film gold [8]. A sample is placed upon a precision x-y translation stage. A small heater beneath the sample is used to control the sample's overall temperature. The microscope uses a swappable LED to illuminate the sample through a fiber-optic coupling. An example of the CNF setup used for the experiments is seen in Figure 2. The SEM image of the same sample is included for reference. The CCD is controlled by the computer by way of

MATLAB (Mathworks Inc.). All the MATLAB routines to acquire and process the data were written in-house. A Kiethley 4200-SCS Parameter Analyser is used to generate the heating and timing signals to the sample and camera.

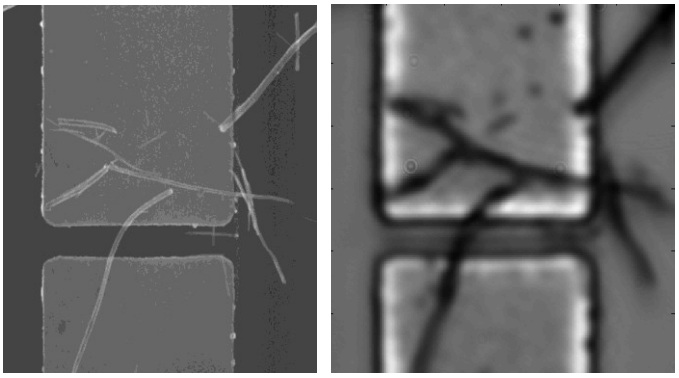

Figure 2: SEM Image of CNF across a two micron gap between ten micron wide gold electrodes at 3500x magnification (left) and optical image of same CNF across gold electrode at 125x magnification (right). The CNF appears wider in the optical image due to diffraction.

In order to measure its thermal properties, the CNF must be locally heated by way of Joule heating. The Joule heating signal is composed of a square current wave. The camera is triggered with a TTL signal. The timing signal passes through a delay generator before reaching the CCD to allow the sample to reach steady state before imaging. The timing diagram is shown in Figure 3.

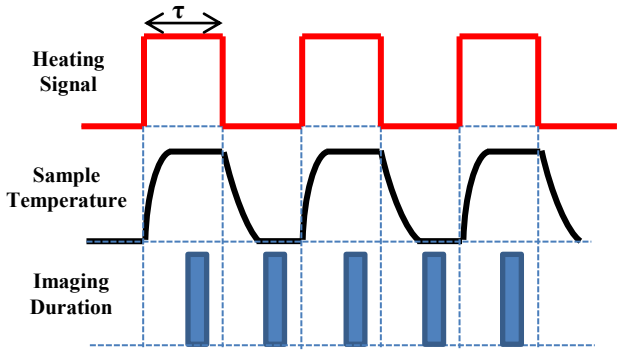

Figure 3: Diagram of the timing sequence with the heating signal, sample temperature, and imaging duration in graphic form. Imaging takes place twice for every cycle, once at a heated time and once at a cool time.

Typical TR coefficients for various materials range from 10^{-4} to 10^{-5} [6]. Because of the weak TR coefficient, it is necessary to measure the reflected intensity of the sample with high precision, both during calibration and during TR imaging. However, CCDs are limited in precision due to the low bit count per pixel and the noise introduced by the analog to digital conversion. In order to reduce this noise, the system averages 2000 images per set. Imaging can be operated in two modes. The full set of images can be averaged together for performing a broad heating calibration, or the images can be taken alternatively as hot and cold images for TR imaging. In order for the TR images to be correlated to temperature, the TR coefficient must first be measured using a broad heating calibration.

HEATING CALIBRATION EXPERIMENT

The calibration of a sample for thermoreflectance experiments is performed by broadly heating the sample. By controlling the temperature of the sample, the change in intensity can be observed. The carbon nanofibers are drop cast onto large gold electrodes atop an insulating SiO_2 layer. The sample is imaged at several elevated temperatures and the increase or decrease in reflectivity is observed. The sample is heated by a Variac-powered ceramic heater under the sample. The sample temperature is recorded using the heater's internal thermocouple or a thermocouple placed on the surface of the sample. In order to remove any water, believed to form an adsorption layer [9], the sample is imaged by starting at the hottest temperature of 220°C. This maximum temperature is limited by the degradation of the gold thin film at higher temperatures. The sample is left to stabilize for approximately one hour at each temperature.

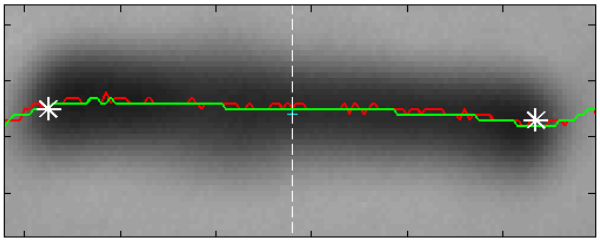

Figure 4: CNF with curve fit minima (green), minima (red), ends (white *), and midline (white) plotted. Total image is approximately two by five microns.

For the calibration procedure, the CNF is imaged atop a large ground gold pad. These CNFs are well away from any edges, preventing diffraction at the edges from affecting the intensity of the CNF. To find a consistent center, the minima location is found along the length of the CNF. This process is illustrated in Figure 4. The center location as measured using the raw minima and a 2^{nd} order curve fit is compared. Also noted are the ends and center of the CNF as determined by an algorithm. To smooth out any noise, the CNF intensity is averaged over a set distance from the center.

An example of the intensity of a cross-section taken along a CNF is shown in Figure 5. The dark CNF atop the gold, 150 nm wide, changes the gold intensity up to a micron away.

Despite the spatial-averaging, any small spatial shift of the CNFs, either from measuring or in the optics, can produce a large change in intensity due to the narrow width of the carbon nanofibers. When imaging the CNFs at elevated temperatures, it was noted that the apparent amount of shifting in each frame increased. It is believed that the change in air density created by air currents is causing the light to diffract differently from image to image. Because of the averaging of 2000 frames, small shifts of the narrow CNF profile would increase the apparent intensity of the CNF.

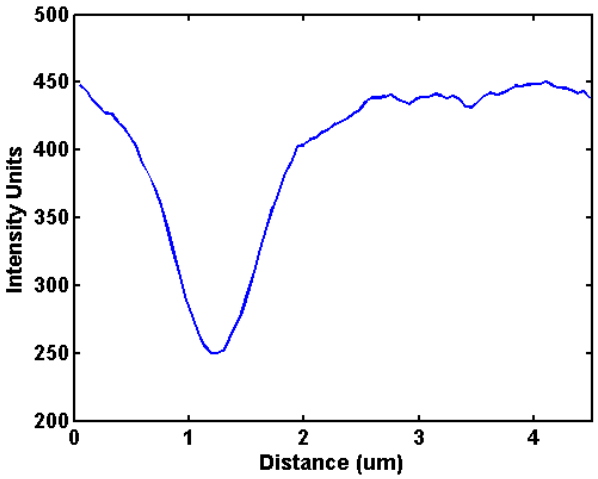

Figure 5: Intensity vs. distances taken along an example CNF. The intensity is in arbitrary units as given by the CCD from 0 to 3000.

It is then necessary to examine and, if possible, to remove this shifting from the calibration images prior to averaging. The shifting could increase the apparent intensity of the CNF and result in an incorrect TR coefficient.

SHIFTING COMPENSATION

The shifting of image frames prevents an accurate calibration. The bright gold underneath the narrow, dark CNFs creates a region of high contrast. Thus, a small shift of only a few pixels will create a large, net increase in CNF intensity when the images are averaged together. In order to remove this shifting, a method to detect the amount of shifting is applied on the raw images. A new average image is created using only those images that have not been significantly shifted.

The amount of shifting is measured by locating the edge of the sample. The edge of the gold layer to SiO_2 creates a peak and valley in the image intensity. By locating the intensity minima along both vertical and horizontal edges, the amount of shifting is measured. While these minima locations do not correspond to the exact edge of the gold and SiO_2, they present reference locations for each image.

Rather than use the raw minima locations along an edge, a 2nd order polynomial curve fit is applied to each edge. The curve fit allows for smoothing of the noise apparent in the individual pixels; hence, providing a more consistent measure for the location of the minimum. The order of the curve fit is not based on the expected diffraction signal. We are currently developing a model to capture the physical effect of the diffraction. The pixels on a horizontal line are used to determine each edge's location in pixels along the vertical edge. The pixels on a vertical line are used along the horizontal edge. An example of this curve fit along the edge is shown in Figure 6. Once the edge locations are determined, a best fit line approximates each edge. The intercept is used as the approximate edge location. Though the curve fit technique increases the amount of computational work required to apply the shifting correction, it also increases the accuracy of the edge-finding method. This edge-finding accuracy helps increase the accuracy of the shifting correction when dealing with a limited number of pixels. The difference between the edge-finding by the local minima and by the curve fit is shown in Figure 7.

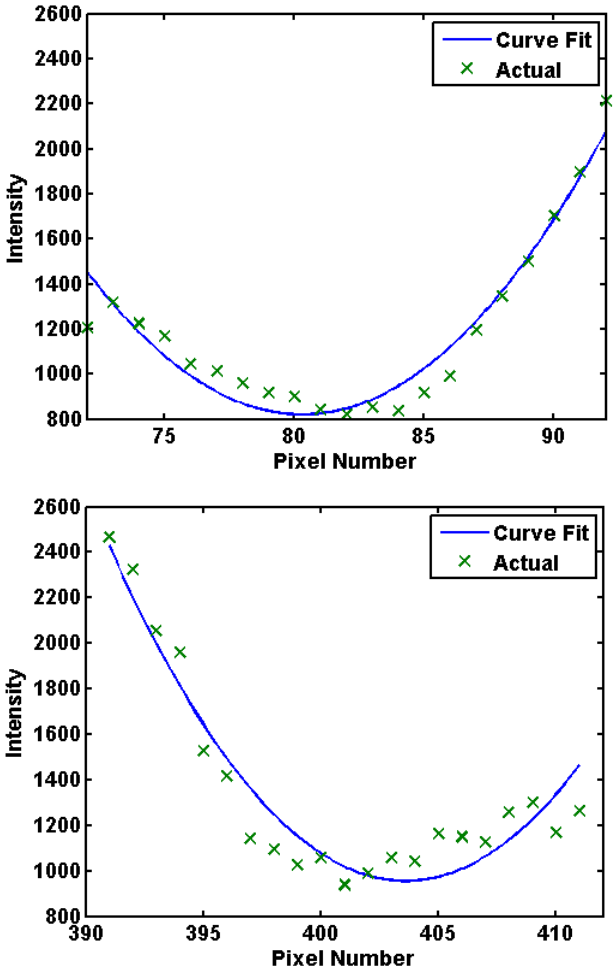

Figure 6a: Vertical Edge. Figure 6b: Horizontal Edge. A second order polynomial curve fit of the edges is taken near the minima locations. These images were taken at an exposure time of 2 ms and a gain of 20.

In order to quantify the shifting effect as a function of the sample temperature, the amount of shifting is measured at the five temperatures used in the calibration, shown in Figure 6. The temperature increase correlates with the amount of shifting which is consistent with the hypothesis that density fluctuations in the air are created by the thermal gradient.

Because the shifting changes as a function of temperature, it is necessary to remove the shifted frames. Once the amount of shifting in each image has been measured, the average image is created using only those frames whose center is within one pixel of the mean. While the shifted images could be corrected and used in the average images, those images are more likely to be blurred. To test the effectiveness and accuracy of this method, the uncompensated, average image is compared to the corrected image at a region of high contrast, such as the edge of the gold and SiO_2. For reference, a slice

from a single frame is included. These are shown in Figure 9. The edge appears much narrower, and the corresponding peak and valley are sharper for the compensated image.

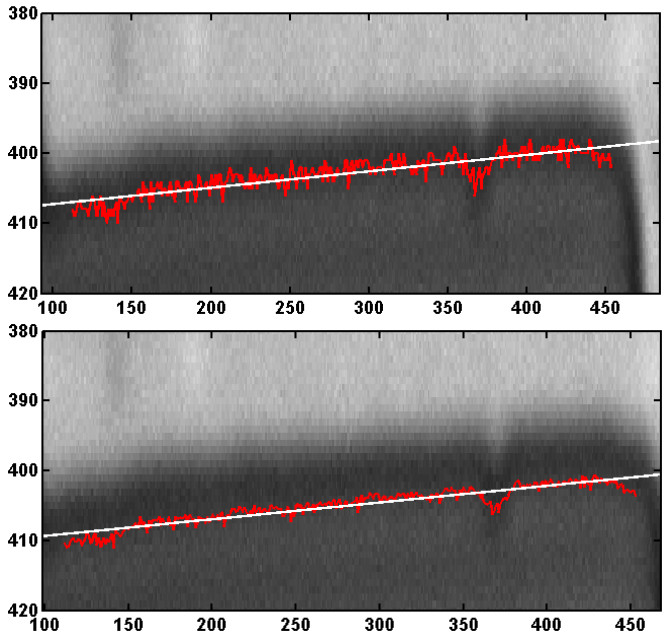

Figure 7: Comparison of gold edge detection techniques. In red are the minima locations, and in white are the linear fits of the minima locations. The minima locations are in the top image and the curve fit locations are below.

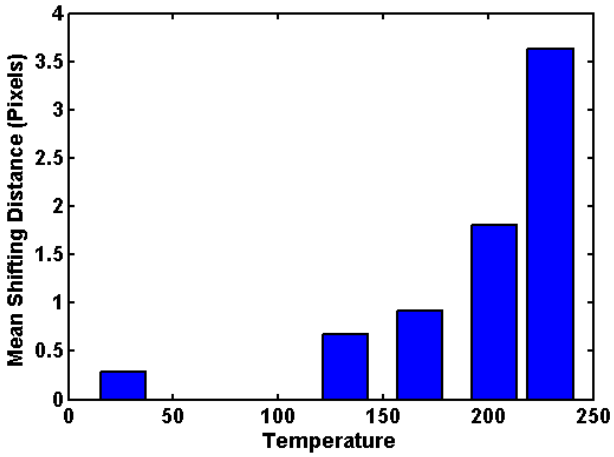

Figure 8: Standard deviation of center location as a function of sample temperature. The largest shifting correlates to a standard deviation of 200 nm.

Once the effectiveness of this routine has been demonstrated, the carbon nanofibers are calibrated using two sets of images: one without shifting compensation and one with shifting compensation. As shown in Figure 10, the normalized intensity of the CNFs increases much less as a function of temperature after the shifting is removed. The TR coefficient is the slope of the best fit line for each set of data. The TR coefficient k_{raw} of the CNFs without the shifting removal is 2.12 x 10^{-4}/K. The TR coefficient k_{comp} with the shifting removal is 7.93 x 10^{-5}/K. This is a decrease of 62%.

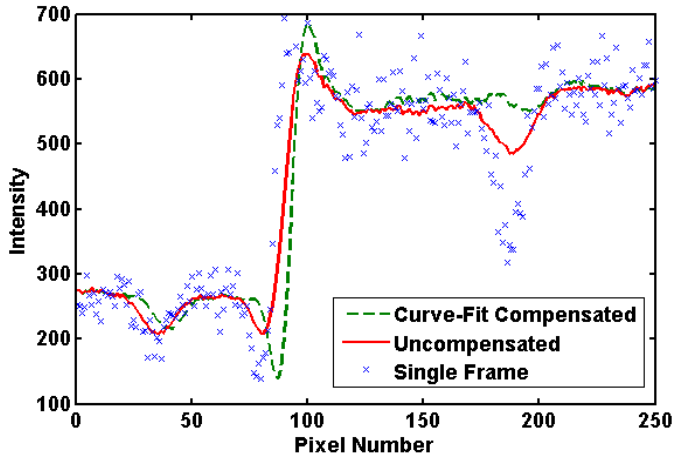

Figure 9: Comparison of edge profiles. The average of all the shifting-compensated images, created using the curve fit edge locations, creates the sharpest edge. The uncompensated average of 2000 frames creates a more dull edge. The noise in a single image is included for reference.

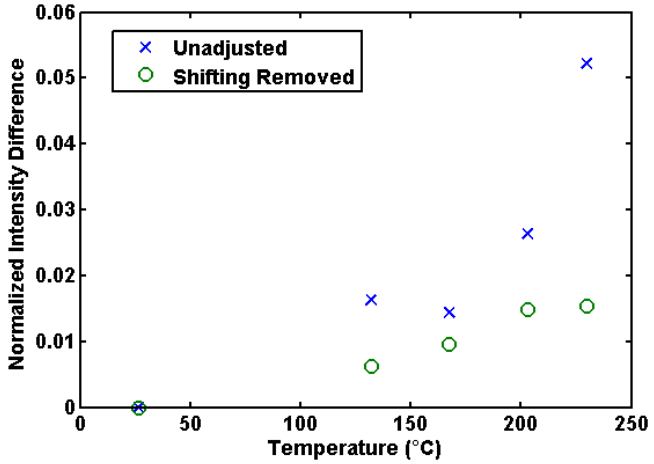

Figure 10: CNF mean intensity as measured using ±5 pixels from center. The intensity gain of the raw images is compared to the images post shifting compensation.

The shifting compensation has a noticeable effect on the CNF intensity. However, the question remains if some of the shifting effect persists. While the shifting in-between frames is being measured and corrected, it is the shifting in each frame that can also cause an increase in CNF intensity. This is akin to the difference between taking two images slightly apart and blurring a photo by moving the camera while the image is being taken. Ultimately, operating the thermoreflectance imaging in a vacuum would be ideal. However, the low focal distance of the microscope objective, needed for a high magnification, as well as the electrical probing system prevents the system from being operating in a vacuum. In order to test the accuracy of our broad calibration, it will be necessary to produce a second TR coefficient from the Joule heating experiments and a heat transfer model.

JOULE HEATING EXPERIMENT

The carbon nanofibers are subject to Joule heating in order to create a local hot spot. The TR signal of the CNF is then compared to the predicted peak temperature using a heat transfer model in order to produce a second estimate of the TR coefficient k_{Joule}.

For the experiments, approximately 150 nm diameter and several microns long CNFs are deposited by drop casting onto a substrate consisting of thin film gold electrodes atop and insulating SiO_2 layer. The CNFs are heated by way of Joule heating using a pulsed, square current wave. By use of an illumination source wavelength close to the cross-point of gold, we minimize gold signal mixing with the CNFs. Furthermore, gold at the chosen wavelength, 505 nm, exhibits a negative TR response with k_{gold} equal to -2.32 x 10^{-5}/K. The CNFs, from our broad heating calibration experiments, have been shown to exhibit a positive TR response. The use of two opposite TR coefficients provides a method to easily measure the temperature of two different materials. Shifting correction is not used on these images as it has been shown that the shifting amount is negligible at non-elevated temperatures.

Prior to imaging, the CNFs were annealed at the test current. This annealing process, as demonstrated by Yamada *et al.*, uses current stressing to decreases the contact resistance [10]. The current stressing uses a constant amount of current, instead of a pulsed square wave, to decrease the contact resistance of the CNF. The CNF was subjected to current densities up to 1.35 MA/cm^2. This is equivalent to 425 µA on a 100 nm diameter CNF with a net electrical resistance of 4 kΩ. These current densities are consistent with previous findings by Suzuki *et al.* [11] and Maeda *et al.* [12]. Suzuki *et al.* found that the peak current density of CNFs were 3 MA/cm^2. Maeda *et al.* determined that the resistance of CNFs was higher in air than vacuum.

To take a full set of images, the hot and cold images are taken alternatively. The frequency of imaging is 20 Hz, or double the frequency of the heating signal, 10 Hz. The camera trigger is delayed from the start of the heating by 25 ms in order to give the sample enough time to reach steady-state. Due to the very small size of the samples, it has been calculated that 25 ms is more than adequate time to reach steady-state. The CNFs are imaged at an exposure time of 18 ms. Longer exposures would increase the amount of blurring. Shorter exposures would decrease the intensity of the already dark CNFs. While the gain on the CCD could be increased to compensate for any decreased intensity, this would increase the noise in each image.

Due to the memory limitations of the computer, the full set of images taken must be broken into smaller chunks. Once these have been sorted, the TR image is produced with the average of the hot and the average of the cold images. The difference between the hot and cold images, divided by the cold image, gives the normalized difference. This is shown in Figure 11. An SEM image is overlaid with the TR in order to show the location of the heating signal on the CNF. The heating of the CNF is in red and yellow. The heating of the gold and SiO_2 is in blue. An optical image combined with the SEM overlay is also provided.

The low pixel count, high noise of the CCD, and the low intensity of the CNFs are all detrimental to the accuracy of the TR imaging. To more accurately extract the peak temperature of the CNF, a 2nd order polynomial fit of the hot spot in the TR image. This fit is taken along the corresponding center location of the CNF in the optical image. This process is repeated for various electrical currents applied across the CNF in ambient conditions.

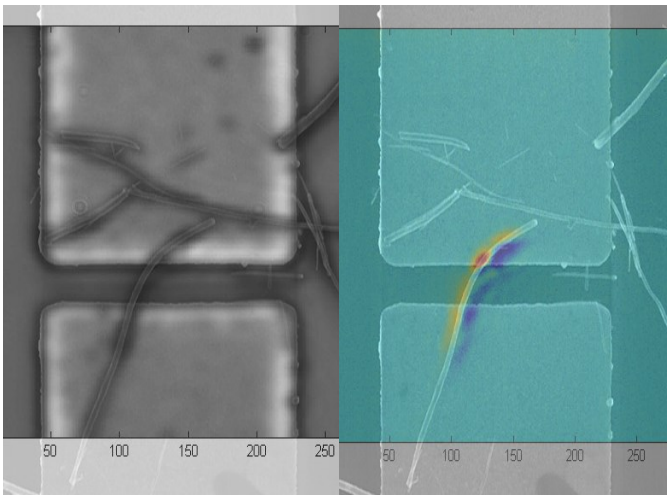

Figure 11: SEM overlay with optical image (left) and SEM overlay with TR image (right). The CNF TR heating signal is in red, and the SiO_2 and gold heating signal is in blue.

The total power being delivered is proportional to current squared.

$$P = I^2R \tag{3}$$

Because of the small size of the CNF, the reflected intensity of the CNF differs from the predicted blackbody absorption and reflection for a large flat surface. The TR response of the CNF is roughly proportional to the total power being delivered to the CNF, shown in Figure 12.

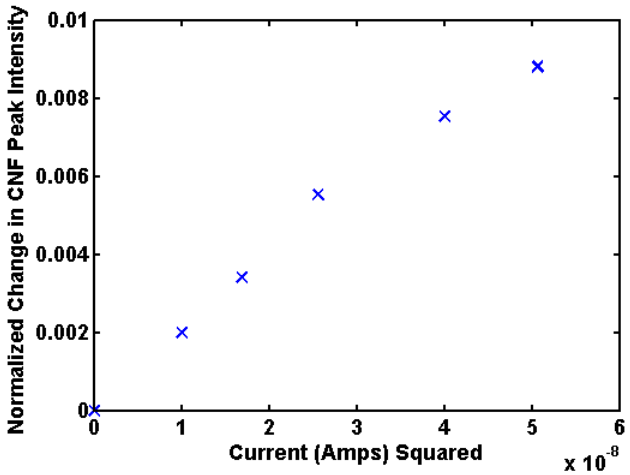

Figure 12: Change in relative CNF peak intensity as a function of current squared. The peak current is equivalent to 225 µA.

However, this change in relative intensity, using the TR coefficient derived from the broad-heating calibration, corresponds to a peak CNF temperature of only 110°C. The expected breakdown temperature is much higher, at 550°C [13]. This discrepancy means that k_{conp} must be too high; a larger TR coefficient k results in a lower temperature change for a fixed change in relative intensity. For comparison, the TR coefficient k_{Joule} will be derived using the TR peak intensity and a heat transfer model.

HEAT TRANSFER MODEL

The peak temperature of the CNF undergoing Joule heating is estimated using a heat transfer model in order to derive the thermoreflectance coefficient k_{Joule}. The model is created by analyzing the heat transfer of the suspended CNF. This model is derived by Fabris *et al.* [14]. Constant properties are assumed throughout. Along the CNF, axial conduction, dissipation to the air, and internal heat generation caused by Joule heating are considered. The CNF temperature is assumed to be 1-D. It is assumed that the heat is conducted by the air from the suspended CNF to the substrate. At the ends, the electrical resistance increases the internal generation. This is a worst case scenario that also simplifies the model. Thermal contact resistance exists between the CNF and the gold electrode, the gold and the SiO_2 insulation layer, and between the SiO_2 and the Si substrate. The thermal contact resistance between the CNF and the gold and thermal conductivity were taken from Yu *et al.* [15].

A differential analysis yields the heat transfer equation similar to a fin,

$$-k\omega \left.\frac{\partial T}{\partial x}\right|_x + \frac{I^2}{\sigma\omega}\Delta x = -k\omega \left.\frac{\partial T}{\partial x}\right|_{x+\Delta x} + \gamma(T - T_{sub})\Delta x \quad (4)$$

where k is the thermal conductivity of the CNF, ω is the cross-sectional area of the CNF, T is the temperature along the CNF, x is the distance from the center, I is the electrical current being delivered to the CNF, σ is the electrical conductivity of the CNF, γ is the heat loss per length along the CNF, and T_{sub} is the temperature of the substrate below the CNF. The boundary conditions must now be considered. The conduction at the end of the CNF, plus the contact heating, are equal to the conduction to the gold.

$$Q_{end} = -k\omega \left.\frac{\partial T}{\partial x}\right|_{x=l} + I^2 R_{e,c} \quad (5)$$

where Q_{end} is the heat being delivered from the CNF to the gold, l is the half length of the CNF, and $R_{e,c}$ is the electrical resistance of the CNF. Thus, the temperature difference between the end of the fiber and the substrate is

$$\Delta T_{end} = Q_{end}/R_{t,c} \quad (6)$$

where $R_{t,c}$ is the thermal contact resistance. The estimation for this resistance is the same used by Yu *et al.* [15] and relies on the effective contact area. The temperature of the substrate below the CNF T_{sub} is dependent on the temperature of the CNF. Thus, a substitution for T_{end}, or the end temperature of the CNF, is used to remove T_{sub} so that the heat transfer equation can be solved. The final form of the heat transfer equation is

$$\frac{\partial^2 \Delta T}{\partial x^2} - a^2 \Delta T = f' \quad (7)$$

where a^2 is the dissipation term, f' is the generation term, and ΔT is the local temperature difference of the CNF and the end. The modified generation term f' is equal to the generation term plus the boundary conditions so that

$$f' = -\frac{I^2}{k\sigma\omega^2} - a^2(Q_{sub}R_{sub} - Q_{end}R_{end}) \quad (8)$$

Thus, ΔT at $x=l$ is zero. The CNF solves to familiar fin equation of

$$\Delta T(x) = \frac{f'}{a^2}\left(1 - \frac{\cosh(ax)}{\cosh(al)}\right) \quad (9)$$

which uses the hyperbolic cosine function. For the four micron long test CNF, the temperature distribution is as shown in Figure 13.

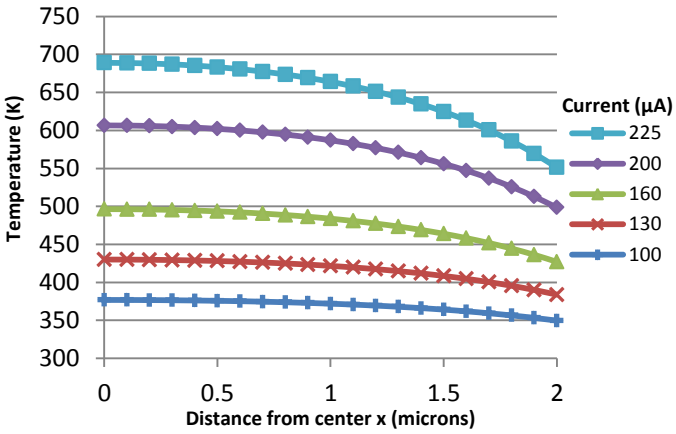

Figure 13: Temperature distribution along CNF with ambient temperature of 300 K.

The model uses theoretical estimates for contact resistance at the fiber end and the heat dissipation to the substrate based on previous work [14, 16]. In an experimental setting, this is expected to vary case by case due to uncontrolled factors. In addition, the thermal conductivity for the CNF was measured by Yu at ambient temperature. As such, the peak temperatures predicted by the model are an indication of the expected temperature distribution and provide a comparison case for the current measurements. The peak temperatures as predicted by the model appear to be consistent, achievable temperatures for CNFs. According to Vignes *et al.*, CNFs begin to breakdown in one atmosphere of air at 720 K and completely at 820 K [13]. In our prior experimental work the CNFs are found to breakdown at current loads slightly above the range tested in this study [17].

In comparing the prediction from the theoretical model to the experimental TR coefficient measurement a discrepancy exists. This discrepancy may be due to the nature of the reflectivity from the small curved surface as well as the two different modes of self-heating. As a result, more work should be done to understand the nature of the diffraction at this scale, the self-heating mechanism and reflectivity from the curved surface.

The thermoreflectance coefficient for CNFs is derived from two different methods. The broad-heating calibration suffers from shifting of separate frames. After compensating for the shifting, the TR coefficient k_{comp} is measured to be 7.93 x 10^{-5}/K. However, it is possible that blurring, created by the shifting, remains and falsely increases the CNF intensity.

After estimating the peak TR temperature with a heat-transfer model, a TR coefficient k_{Joule} is derived from the peak TR response of the CNFs undergoing Joule heating. These responses are plotted against each other in Figure 14.

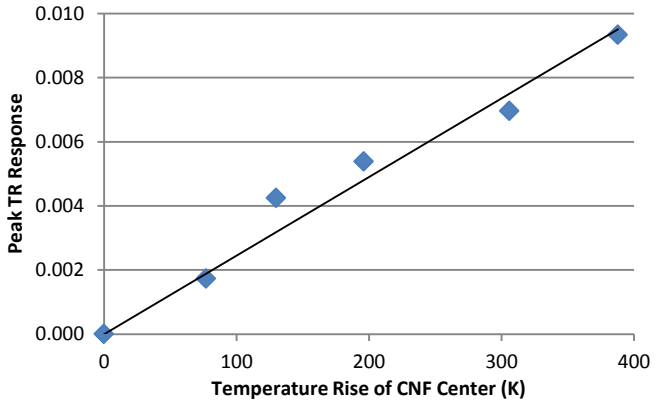

Figure 14: Peak TR response of the CNF vs model temperature. The slope of the best-fit line is 2.45 x 10^{-5}/K.

The slope of this line, equal to the TR coefficient $k_{Joule.}$, is 2.45 x 10^{-5}/K. This k_{Joule} is three times lower than k_{comp}. It is assumed that the broad-heating calibration of the CNFs is unreliable due to the shifting produced by air currents. The heat-transfer model used to produce the TR coefficient k_{Joule} appears to accurately capture the breakdown temperature of the CNF. This indicates that the k_{CNF} is on the order of 10^{-5} and close to k_{gold}. Therefore, the TR imaging of CNFs requires an illumination wavelength even closer to the cross-point than is currently in use.

CONCLUSIONS

The thermoreflectance behavior of carbon nanofibers is investigated successfully. The cross-point of gold, with a well-documented TR response, minimizes signal mixing with a novel material to allow for imaging at the sub-micron level. The experimental procedures to achieve a calibration are developed and utilized. A method to measure and correct for shifting during the calibration is used with limited success. A heat transfer model is used to evaluate the TR coefficient from a Joule-heating experiment. The positive thermoreflectance coefficient of carbon nanofibers is measured to be on the order of 10^{-5} with the two coefficients agreeing within a factor of three. Future experiments are suggested to measure CNFs while in vacuum and with more precision in imaging and illumination source.

ACKNOWLEDGEMENTS

The authors are thankful to Chris Cardenas, Sahida Kureshi, and Toshishige Yamada for their contributions and support.

REFERENCES

[1] "2012 International Technology Roadmap for Semiconductors," 2012. [Online]. Available: www.itrs.net.

[2] A. V. Melechko, V. I. Merkulov, T. E. McKnight, M. A. Guillorn, K. L. Klein, D. H. Lowndes and M. L. Simpson, "Vertically aligned carbon nanofibers and related structures: Controlled synthesis and directed assembly," *Journal of Applied Physics,* vol. 97, no. 4, p. 041301, 2005.

[3] J. Christofferson, K. Maize, Y. Ezzahri, J. Shabani, X. Wang and A. Shakouri, "Microscale and Nanoscale Thermal Characterization Techniques," *Journal of Electronic Packaging,* vol. 130, no. 4, p. 041101, 2008.

[4] D. J. Yang, Q. Zhang, G. Chen, S. F. Yoon, J. Ahn, S. G. Wang, Q. Zhou, Q. Wang and J. Q. Li, "Thermal Conductivity of Multiwalled Carbon Nanotubes," *Physical Review B,* vol. 66, no. 16, p. 165440, 2002.

[5] A. Balandin, S. Ghosh, W. Bao, I. Calizo, D. Teweldebrhan, F. Miao and C. N. Lau, "Superior Thermal Conductivity of Single-Layer Graphene," *Nano Letters,* vol. 8, no. 3, pp. 902-907, 2008.

[6] M. G. Burzo, P. L. Komarov and P. E. Raad, "Optimized Thermo-Reflectance System for Measuring the Thermal Properties of Thin-Films and Their Interfaces," in *22nd SEMI-THERM Symposium*, Dallas, USA, 2006.

[7] A. Beran, "The Reflectance Behaviour of Gold at Temperatures up to 500C," *Tschermaks Mineralogische und Petrographische Mitteilungen (TMPM),* vol. 34, no. 3, pp. 211-215, 1985.

[8] C. Cardenas, D. Fabris, S. Tokairin, F. Madriz and C. Y. Yang, "Thermoreflectance Measurement of Temperature and Thermal Resistance of Thin Film Gold," *Journal of Heat Transfer,* vol. 134, no. 11, p. 111401, 2012.

[9] D. Fabris, C. Cardenas, S. Tokairin, P. Wilhite and C. Yang, "Thermoreflectance Small Scale Temperature Measurement Under Ambient Conditions," in *9th International Conference on Heat Transfer*, Malta, July 2012.

[10] T. Yamada, T. Saito, M. Suzuki, P. Wilhite, X. Sun, N. Akhavantafti, D. Fabris and C. Y. Yang, "Tunneling between carbon nanofiber and gold electrodes," *Journal of Applied Physics,* vol. 107, p. 044304, 2010.

[11] M. Suzuki, Y. Ominami, Q. Ngo, C. Y. Yang, A. M.

Cassell and J. Li, “Current-Induced Breakdown of Carbon Nanofibers,” *Journal of Applied Physics,* vol. 101, no. 11, p. 114307, 2007.

[12] S. Maeda, P. Wilhite, N. Kanzaki, T. Yamada and C. Y. Yang, “Change in carbon nanofiber resistance from ambient to vacuum,” *AIP Advances,* vol. 1, no. 2, p. 022102, 2011.

[13] A. Vignes, O. Dufaud, L. Perrin, D. Thomas, J. Bouillard, A. Janès and C. Vallières, “Thermal ignition and self-heating of carbon nanotubes: From thermokinetic study to process safety,” *Chemical Engineering Science,* vol. 64, no. 20, pp. 4210-4221, 2009.

[14] D. Fabris, H. Kitsuki, T. Yamada, X. Sun, J. G. Cruz and C. Y. Yang, “Temperature Modeling for Carbon Nanofiber Breakdown,” in *Proceedings of ASME Summer Heat Transfer Conference*, Jacksonville, USA, 2008.

[15] C. Yu, S. Saha, J. Zhou, L. Shi, A. Cassel, B. Cruden, Q. Ngo and J. Li, “Thermal contact resistance and thermal conductivity of a carbon nanofiber,” *Journal of Heat Transfer,* vol. 128, no. 3, pp. 234-239, 2006.

[16] V. Bahadur, J. Xu, Y. Liu and T. S. Fisher, “Thermal resistance of nanowire-plane interfaces,” *Journal of Heat Transfer,* vol. 127, no. 6, pp. 664-668, 2004.

[17] T. Yamada, T. Saito, D. Fabris and C. Y. Yang, “Electrothermal Analysis of Breakdown in Cabron Nanofiber Interconnects,” *IEEE Electron Device Letters,* vol. 30, no. 5, pp. 469-471, 2009.